Uncertainties in O3 concentrations simulated by CMAQ over Japan using four chemical mechanisms

Kitayama, Kyo
Morino, Yu
Yamaji, Kazuyo
Chatani, Satoru

(Citation)
Atmospheric Environment,198:448-462

(Issue Date)
2019-02-01

(Resource Type)
journal article

(Version)
Version of Record

(URL)
https://hdl.handle.net/20.500.14094/90005571

Atmospheric Environment 198 (2019) 448–462

Contents lists available at ScienceDirect

Atmospheric Environment

journal homepage: www.elsevier.com/locate/atmosenv

Uncertainties in O_3 concentrations simulated by CMAQ over Japan using four chemical mechanisms

Kyo Kitayama[a,*], Yu Morino[a], Kazuyo Yamaji[b], Satoru Chatani[a]

[a] National Institute for Environmental Studies, Onogawa 16-2, Tsukuba, Ibaraki, 3058506, Japan
[b] Kobe University, Fukaeminamimachi 5-1-1, Higashinada-ku, Kobe, Hyogo, 6580022, Japan

ARTICLE INFO

Keywords:
O_3
CMAQ
Chemical mechanism
Process analysis

ABSTRACT

Uncertainty was evaluated in four chemical mechanisms pertaining to O_3 concentrations predicted over Japan by the Community Multiscale Air Quality Model (CMAQ) to investigate factors contributing to model overestimation of O_3 concentration. The model setting and meteorological and emissions input data were obtained from a Japanese model inter-comparison project, Japan's Study for Reference Air Quality Modeling (J-STREAM). The compared gas-phase chemical mechanisms included the Carbon Bond Mechanism (CB05TUCL), Regional Atmospheric Chemical Mechanism (RACM2), and two mechanisms developed by the State Air Pollution Research Center (SAPRC), namely SAPRC07TC and SAPRC99. The O_3 concentrations produced by CB05TUCL were low compared to those from SAPRC07TC. The RACM2 concentrations were similar to those from SAPRC07TC over inland Japan and lower over the sea. The concentrations from SAPRC99 were higher than those from SAPRC07TC in urban areas and lower in other areas. At most of the monitoring sites in Japan, the modeled O_3 concentrations were higher than those from observations. Module overestimation can be ranked in the order of SAPRC99 > SAPRC07TC > RACM2 > CB05TUCL for urban sites and SAPRC07TC > SAPRC99 > RACM2 > CB05TUCL for rural sites. The concentration differences between the chemical mechanisms were within 10 ppb, whereas those between the observed and simulated O_3 concentrations reached 40 ppb. Differences in O_3 concentrations between the chemical mechanisms accounted for only a part of the model overestimation, while the rest remained unexplained. To investigate factors influencing the differences in O_3 concentration between the chemical mechanisms, domain- and 10-vertical-layer-average hourly integrated process rates (IPRs) and integrated reaction rates (IRRs) were calculated using process analysis in CMAQ. The O_3 chemical IPRs from SAPRC07TC were higher than those from CB05TUCL and RACM2. The SAPRC99 IPRs were higher than those from SAPRC07TC in urban areas and lower in other areas. The IRR differences in the chemical mechanisms showed that IRRs for the O_3 and NO reactions were responsible for the differences in the O_3 chemical IPR. The coefficients of determination between the O_3 chemical process IPR and IRR differences in the chemical mechanisms were highest for the HO_2-NO reaction in CB05TUCL and SAPRC99 and the RO_2-NO reaction in RACM2. Differences in reaction rate constants and lumped volatile organic compounds may have caused some of the differences in O_3 production between the chemical mechanisms.

1. Introduction

Tropospheric O_3 air pollution can lower crop yield and damage human health (US EPA, 2006; Yang and Omaye, 2009; Nawahda et al., 2013; Tang et al., 2014; Yamaguchi et al., 2014). Air quality models can be effective tools for predicting pollutant concentrations and developing effective air pollution mitigation policies. However, recent model studies have shown that model-simulated O_3 is over-predicted in East Asia and Japan (Liu et al., 2010; Morino et al., 2010; Li et al., 2012; Chatani et al., 2015; Trieu et al., 2017). Suitable input datasets and model configuration settings must be chosen to enhance model performance. Thus, a Japanese model inter-comparison project, Japan's Study for Reference Air Quality Modeling (J-STREAM), was established to evaluate various uncertainties and clarify appropriate model settings (Chatani et al., 2018b). This study formed part of J-STREAM and focused on uncertainties in the O_3 concentrations associated with the choice of chemical mechanism, which determines the gas-phase chemical reactions, rate constants, and chemical compounds used in the model.

Uncertainty surrounding the influence of chemical mechanisms on

* Corresponding author.
E-mail address: kitayama.kyo@nies.go.jp (K. Kitayama).

https://doi.org/10.1016/j.atmosenv.2018.11.003
Received 3 April 2018; Received in revised form 21 October 2018; Accepted 5 November 2018
Available online 08 November 2018

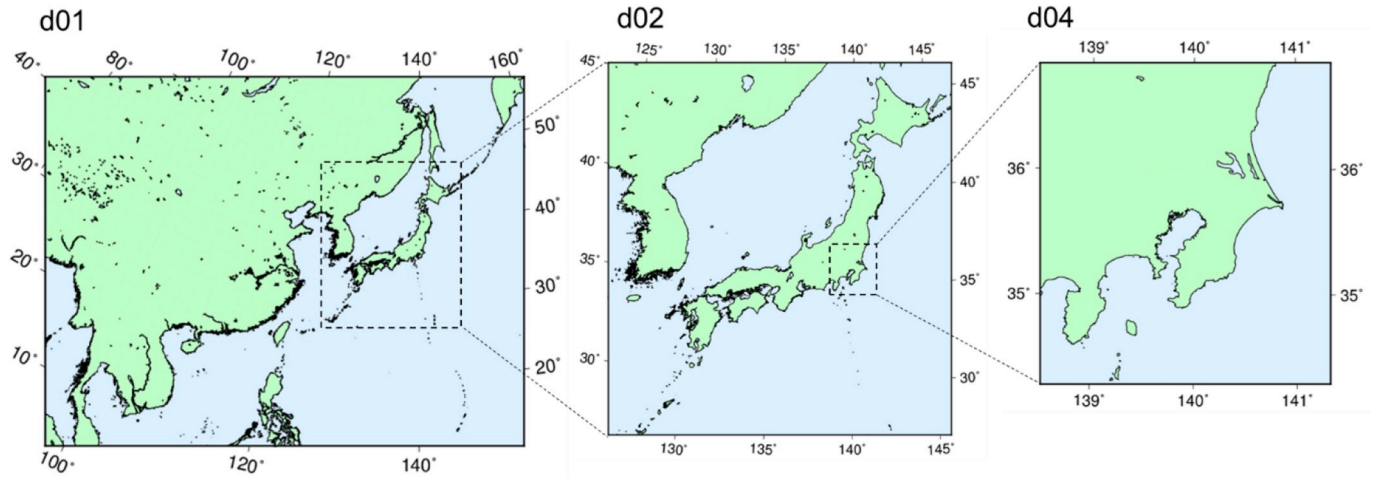

Fig. 1. Domains of the Community Multiscale Air Quality Model simulation in this study.

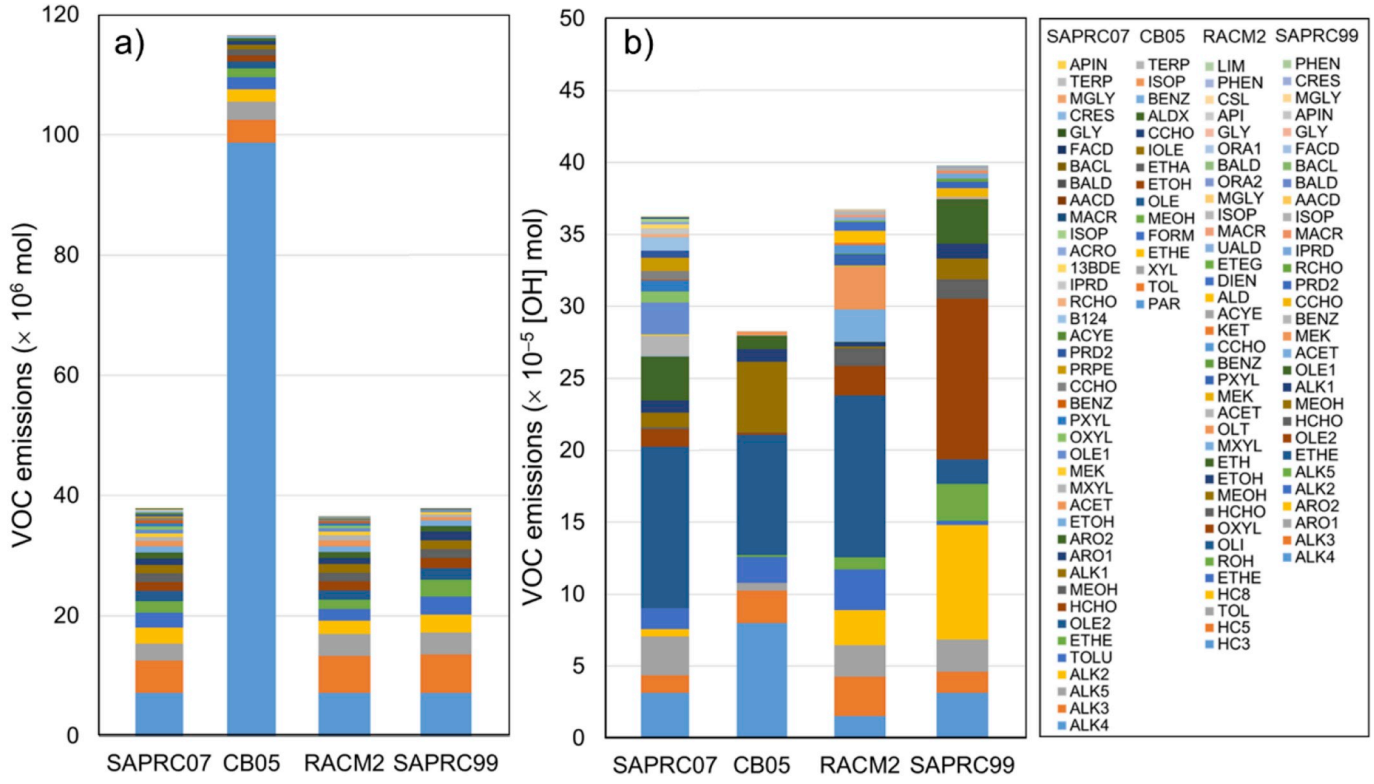

Fig. 2. Emissions of anthropogenic volatile organic compound (VOC) species in the four chemical mechanisms. a) VOC emissions. b) VOC emissions weighted by reaction rate coefficients for OH-reactions. Definitions of abbreviations of chemical compounds in the legend are summarized in Table 1.

O_3 concentrations has been evaluated in numerous studies through model sensitivity tests and inter-comparisons. Sarwar et al. (2013) compared the Regional Atmospheric Chemical Mechanisms 2 (RACM2) module to the Carbon Bond with updated toluene chemistry (CB05TU) module in a simulation over the USA and showed that the mean surface O_3 concentration predicted by RACM2 was 0–12% greater than that predicted by CB05TU. Knote et al. (2015) found a 4 ppb uncertainty in the O_3 concentrations produced by multiple chemical mechanisms from model simulations over the USA and Europe. Cai et al. (2011) reported that O_3 predictions from the mechanism developed by the State Air Pollution Research Center (SAPRC07TC) were lower than those from SAPRC99 in high O_3–concentration areas in simulations over California. Yu et al. (2010) simulated O_3 concentration using CB4, CB05, and SAPRC99 and concluded that SAPRC99 generated the highest concentration and poorest performance for the predictions shown in the USA. However, few comparison studies have been performed for chemical mechanisms in East Asia. A better understanding of chemical mechanism uncertainty in East Asia is needed for precise model evaluation and simulation predictions.

To evaluate the chemical mechanism uncertainty in Japan, O_3 concentrations were simulated using the Community Multiscale Air Quality (CMAQ; Byun and Schere, 2006) model with four chemical mechanisms: CB05TUCL, RACM2, SAPRC07TC, and SAPRC99. Process analysis (Gipson, 1999) was further conducted to evaluate the influence of the chemical processes and reactions on chemical mechanism uncertainty.

Table 1
Abbreviations of volatile organic compound species in the four chemical mechanisms.

Chemical mechanism	Species	Description
SAPRC07, CB05, RACM2, SAPRC99	TOLU	Toluene
	ETHE	Ethene
	HCHO	Formaldehyde
	MEOH	Methanol
	ETOH	Ethanol
	ACET	Acetone
	MXYL	M-xylene
	OXYL	O-xylene
	PXYL	P-xylene
	MEK	Ketones and other non-aldehyde oxygenated products whose kOH are between 5×10^{-13} and 5×10^{-12} $cm^3\,mol^{-2}\,s^{-1}$ (based on methyl ethyl ketone)
	BENZ	Benzene
	CCHO	Acetaldehyde
	PRPE	Propene
	ACYE	Acetylene
	ACRO	Acrolein
	ISOP	Isoprene
	MACR	Methacrolein
	AACD	Acetic acid
	BALD	Aromatic aldehyde (mechanism based on benzaldehyde)
	FACD	Formic acid
	GLY	Glyoxal
	MGLY	Methylglyoxal
	APIN	Pinene
SAPRC07, SAPRC99	ALK1	Alkanes and other non-aromatic compounds that react only with OH having kOH (OH radical rate constant) $< 5 \times 10^2$ $ppm^{-1}\,min^{-1}$ (primarily ethane)
	ALK2	The same as ALK1 but with kOH values between 5×10^2 and 2.5×10^3 $ppm^{-1}\,min^{-1}$ (primarily propane and acetylene)
	ALK3	The same as ALK1 but with kOH values between 2.5×10^3 and 5×10^3 $ppm^{-1}\,min^{-1}$
	ALK4	The same as ALK1 but with kOH values between 5×10^3 and 1×10^4 $ppm^{-1}\,min^{-1}$
	ALK5	The same as ALK1 but with kOH values $> 1 \times 10^4$ $ppm^{-1}\,min^{-1}$
	ARO1	Aromatics with kOH $< 2 \times 10^4$ $ppm^{-1}\,min^{-1}$
	ARO2	Aromatics with kOH $> 2 \times 10^4$ $ppm^{-1}\,min^{-1}$
	OLE1	Alkenes with kOH $< 7 \times 10^4$ $ppm^{-1}\,min^{-1}$
	OLE2	Alkenes with kOH $> 7 \times 10^4$ $ppm^{-1}\,min^{-1}$
	PRD2	Ketones and other non-aldehyde oxygenated products whose kOH $> 5 \times 10^{-12}$ $cm^3\,mol^{-2}\,s^{-1}$ (based on higher ketones formed from alkanes)
	RCHO	Lumped C_3 + aldehydes (mechanism based on propionaldehyde)
	IPRD	Lumped isoprene product species (Carter and Atkinson, 1996)
	BACL	Biacetyl
SAPRC07	CRES	Phenols and cresols (mechanism based on o-cresol)
	B124	1,2,4-Trimethylbenene
	13BDE	1,3-Butadiene
	TERP	Terpenes
CB05	PAR	Paraffin carbon bond (C-C)
	TOL	Toluene and other monoalkyl aromatics
	XYL	Xylene and other polyalkyl aromatics
	FORM	Formaldehyde
	OLE	Terminal olefin carbon bond (R-C=C)
	ETHA	Ethane
	IOLE	Internal olefin carbon bond (R-C=C-R)
	ALDX	Propionaldehyde and higher aldehydes
	TERP	Terpene
RACM2	HC3	Alkanes, esters, and alkynes with kOH $< 3.4 \times 10^{-12}$ $cm^3\,s^{-1}$
	HC5	Alkanes, esters, and alkynes with kOH between 3.4×10^{-12} and 6.8×10^{-12} $cm^3\,s^{-1}$
	HC8	Alkanes, esters, and alkynes with kOH $> 6.8 \times 10^{-12}$ $cm^3\,s^{-1}$
	TOL	Toluene and less reactive aromatics
	ROH	C_3 and higher alcohols
	OLI	Internal alkenes
	ETH	Ethane
	OLT	Terminal alkenes
	MEK	Methyl ethyl ketone
	KET	Ketones
	ALD	C_3 and higher aldehydes
	DIEN	Butadiene and other anthropogenic dienes
	ETEG	Ethylene glycol
	UALD	Unsaturated aldehydes
	MGLY	Methylglyoxal and other alpha-carbonyl aldehydes
	ORA1	Formic acid
	ORA2	Acetic acid and higher acids
	API	Alpha-pinenes and other cyclic terpenes with one double bond
	CSL	Cresol and other hydroxy substituted aromatics
	PHEN	Phenol
	LIM	D-limonene and other cyclic diene-terpenes
SAPRC99	CRES	Cresols
	PHEN	Phenols

Chemical species defined by Carter (2010a) for SAPRC07, Yarwood et al. (2005) for CB05, Goliff et al. (2013) for RACM2, and Carter (2000) for SAPRC99.

2. Methods

The model settings, computational domains, and target periods of this study were based on standard J-STREAM methods (Chatani et al., 2018b). This section includes a brief description of the standard model settings and settings that differed from the standard.

2.1. Model settings and study period

Standard J-STREAM meteorological data were used as meteorological inputs. These standard data were generated by the Weather Research and Forecasting Model version 3.7.1 (Skamarock et al., 2008) using the National Centers for Environmental Prediction (NCEP) Final Operational Model Global Tropospheric Analyses (ds083.2) (NCEP, 2000) and Real-Time, Global, Sea Surface Temperature (RTG_SST_HR) analysis (Gemmill et al., 2007) for the initial and boundary conditions. The O_3 concentration was calculated using CMAQ version 5.0.2 (Byun and Schere, 2006). The target domains included the d01, d02, and d04 J-STREAM domains (Fig. 1). The d01 area covers East and Southeast Asia at a horizontal grid size of 45 km, the d02 area covers Japan and features a 15 km grid, and the d04 area covers the Kanto region, which includes urban Tokyo; the d04 grid resolution is 5 km. Boundary concentrations were obtained from Chemical Atmospheric Circulation Model for the Study of Atmospheric Environment and Radiative Forcing results (Sudo et al., 2002) using the Hemispheric Transport of Air Pollution 2 (Huang et al., 2017) for d01, while the outer domain results were used for d02 and d04. The vertical dimension consists of 30 layers between the ground and 100 hPa. The study period spanned July 22 to August 10, 2013, which, of the five J-STREAM target periods, constitutes the summer season. The CMAQ calculation was performed from July 1, 2013, which includes the run-up period for the target calculation.

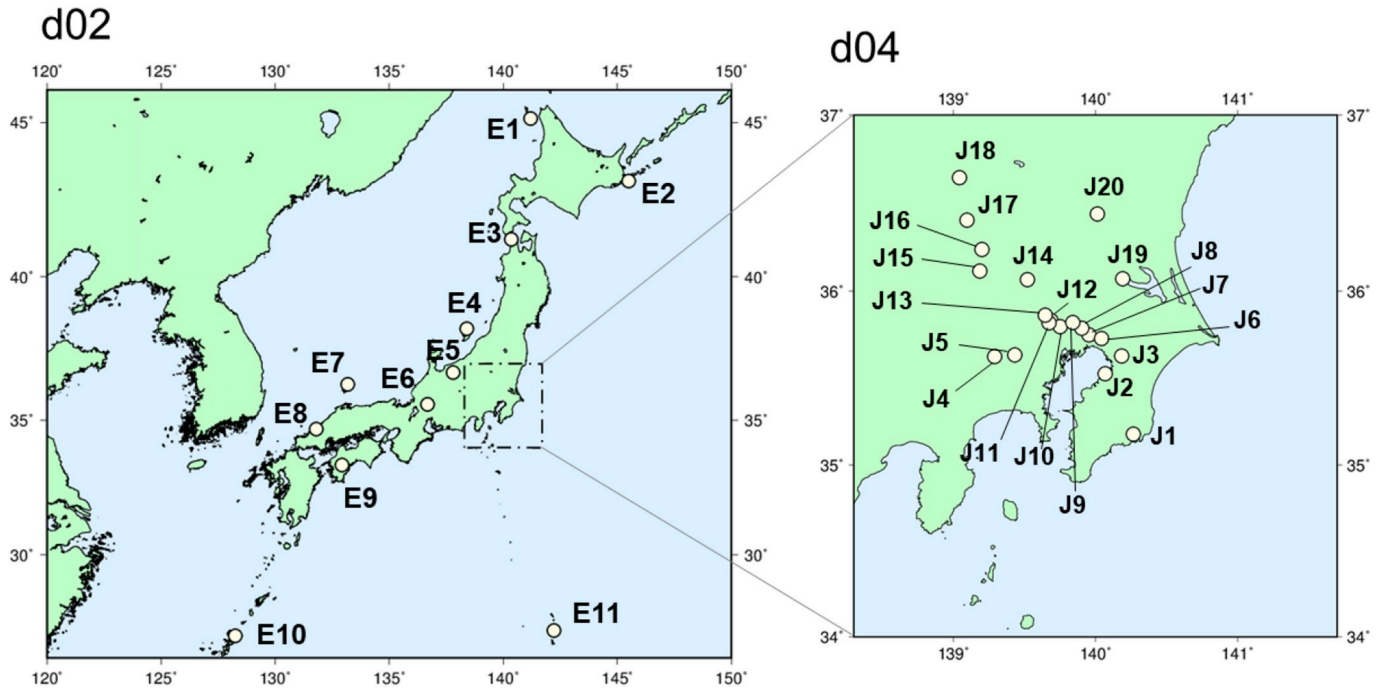

Fig. 3. Site locations of the observational data used for model result comparisons. E1–E11 are Acid Deposition Monitoring Network in East Asia sites, and J1–J20 are automatic monitoring sites.

2.2. Chemical mechanisms

Four gas-phase chemical mechanisms were used in CMAQ calculations to evaluate O_3 concentration uncertainties between the chemical mechanisms. The selected mechanisms included CB05TUCL (Sarwar et al., 2008; Whitten et al., 2010), RACM2 (Goliff et al., 2013), SAPRC07TC (Carter, 2010a; b), and SAPRC99 (Carter, 2000, Carter et al., 2000). These chemical mechanisms cover almost all of the mechanisms included in CMAQ. CB05TUCL is based on CB05 (Yarwood et al., 2005) and was updated with toluene reactions. The mechanism consists of 205 reactions and includes 27 photolytic reactions and 80 gas-phase chemical species. RACM2 contains 363 reactions, including 33 photolytic reactions involving 128 chemical species. SAPRC07TC consists of 689 reactions and includes 55 photolytic reactions and 150 chemical species. SAPRC99 consists of 224 reactions, including 30 photolytic reactions and 89 chemical species.

The AERO6 aerosol chemical scheme was used for CB05TUCL, RACM2, and SAPRC07TC. For SAPRC99, the AERO5 aerosol chemical scheme was selected to investigate the influence of the aerosol chemical scheme on O_3 concentration. However, the aerosol scheme appeared to exert little influence on O_3 concentration, which is part of the gas-phase chemical cycle.

2.3. Emissions

The base emissions datasets used as model input are described by Chatani et al. (2018b). For the emissions from Japan, Hemispheric Transport of Air Pollution version 2.2 (Janssens-Maenhout et al., 2015) was used for anthropogenic sources and ships. For the emissions from Japan, the Japan Auto-Oil Program (JATOP) emissions inventory database was used for anthropogenic sources. Vehicle emissions were estimated by the JATOP emissions inventory–vehicle emissions estimation model (Chatani et al., 2011), and other anthropogenic emissions were derived from updated activity databases for 2013. For open biomass burning, Global Fire Emissions Database version 4.1 (Van der Werf et al., 2017) was used. SO_2 emissions from four volcanoes (Asamayama, Asosan, Sakurajima, and Miyakejima) in Japan were obtained from the Japan Meteorological Agency (2017), and those from two other volcanoes (Satsuma-Iojima and Suwanosejima) were obtained from AeroCom (Diehl et al., 2012). The other volcanic SO_2 emissions were obtained from Aerosol Comparisons Observations and Models (AeroCom; Diehl et al., 2012). Hourly biogenic volatile organic compound (VOC) emissions both outside of and within Japan were estimated by the Model of Emissions of Gases and Aerosols from Nature (MEGAN) version 2.1 (Guenther et al., 2012). However, the biogenic VOC emissions of MEGAN were reported to be over-estimated compared to those of the Biogenic Emissions Inventory System in previous studies (Carlton and Baker, 2011; Hogrefe et al., 2011). In ad13dition, Chatani et al. (2018a) developed a new database of vegetation types and emissions factors for estimating biogenic VOC emissions. These authors found that a new database resulted in lower emissions than the default MEGAN database did. Therefore, these studies imply that biogenic VOC emissions used in this study may be overestimated.

In this study, the chemical species emissions included in the VOCs had to be rearranged to correspond to the species used in the four chemical mechanisms. The emissions of individual VOC species included in the emissions inventory databases were allocated into the lumped species defined in the four chemical mechanisms following the speciation table provided by Carter (2016). The aggregated amounts of anthropogenic VOC emissions in the four chemical mechanisms normalized by SAPRC07TC emissions are shown in Fig. 2. The abbreviations of volatile organic compound species used in Fig. 2 are listed in Table 1. The large paraffin (PAR) emissions in CB05TUCL arose from differences between the chemical mechanisms in the handling of lumped species. For CB05, the number of carbon bonds in the chemical species was counted toward the PAR emissions, which caused increased PAR emissions in CB05TUCL compared to those in the other chemical mechanisms. However, the CB05TUCL VOC emissions were the lowest among the four chemical mechanisms when they were weighted by reaction rate coefficients for OH-reactions. This indicates that the reactivities of the VOCs in CB05TUCL were lower than those in the other chemical mechanisms.

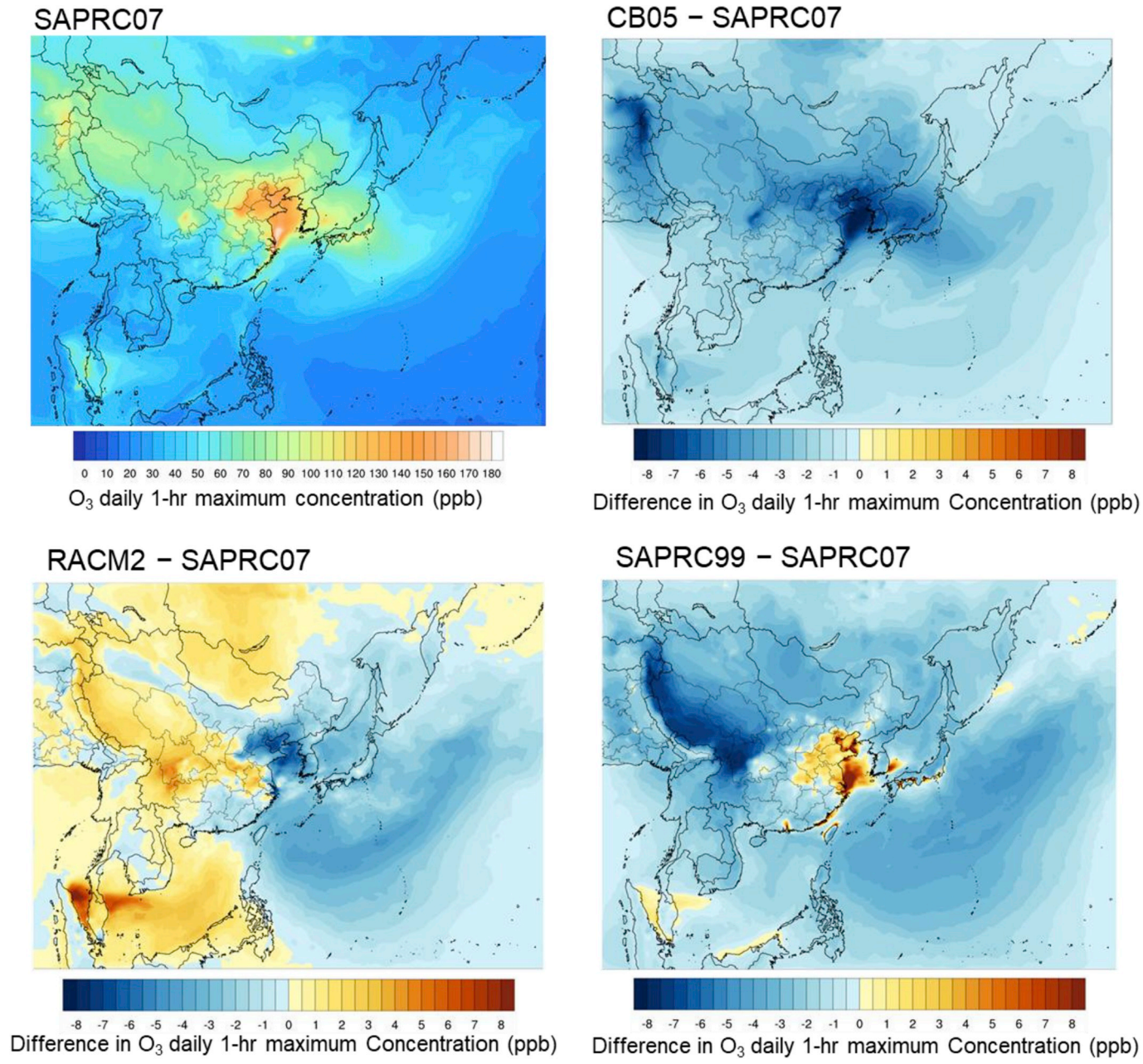

Fig. 4. Distributions of daily 1 h maximum O_3 concentrations averaged over the target season and differences between the concentrations produced by the chemical mechanisms, shown over d01.

2.4. Process analysis

Process analysis (Gipson, 1999), including integrated process rates (IPRs) and integrated reaction rates (IRRs), was used to evaluate uncertainties in simulated O_3 concentrations in the four chemical mechanisms. IPRs encompass integrated rates of change in O_3 concentrations due to advection, diffusion, dry deposition, clouds, and chemical reaction processes. Cloud processes include chemical reactions in the liquid phase, convective transport, and wet deposition. IRRs include all of the reaction rates in each mechanism. The IRRs of reactions related to the O_3 concentration can be used to evaluate reactions that factor into the concentration differences between the chemical mechanisms. Zhang et al. (2009) used process analysis on CMAQ simulations in the USA to show that transport was the most influential O_3 process in the planetary boundary layer. Khiem et al. (2010) applied process analysis for CMAQ O_3 simulation in urban areas in Japan and concluded that ground-level O_3 was enhanced by vertical mixing and depleted by dry deposition and chemical processes.

2.5. Observation datasets

The observation datasets were obtained by the Acid Deposition Monitoring Network in East Asia (EANET) over d02; EANET data details are given in EANET (2014). Gaseous pollutants, including O_3, were monitored every hour by automatic samplers using absorptiometry, coulometry, ultraviolet absorption, or chemiluminescent methods. The monitoring sites used for comparison in this study are shown in Fig. 3. E8 was an urban site, and the other EANET sites were rural or remote. For d04, automatic monitoring datasets from the Japanese Ministry of the Environment were used for verification. The collection interval and chemical species used in this study matched the EANET data, and the d04 sites were urban or rural. Further data details are described in Chatani et al. (2018b).

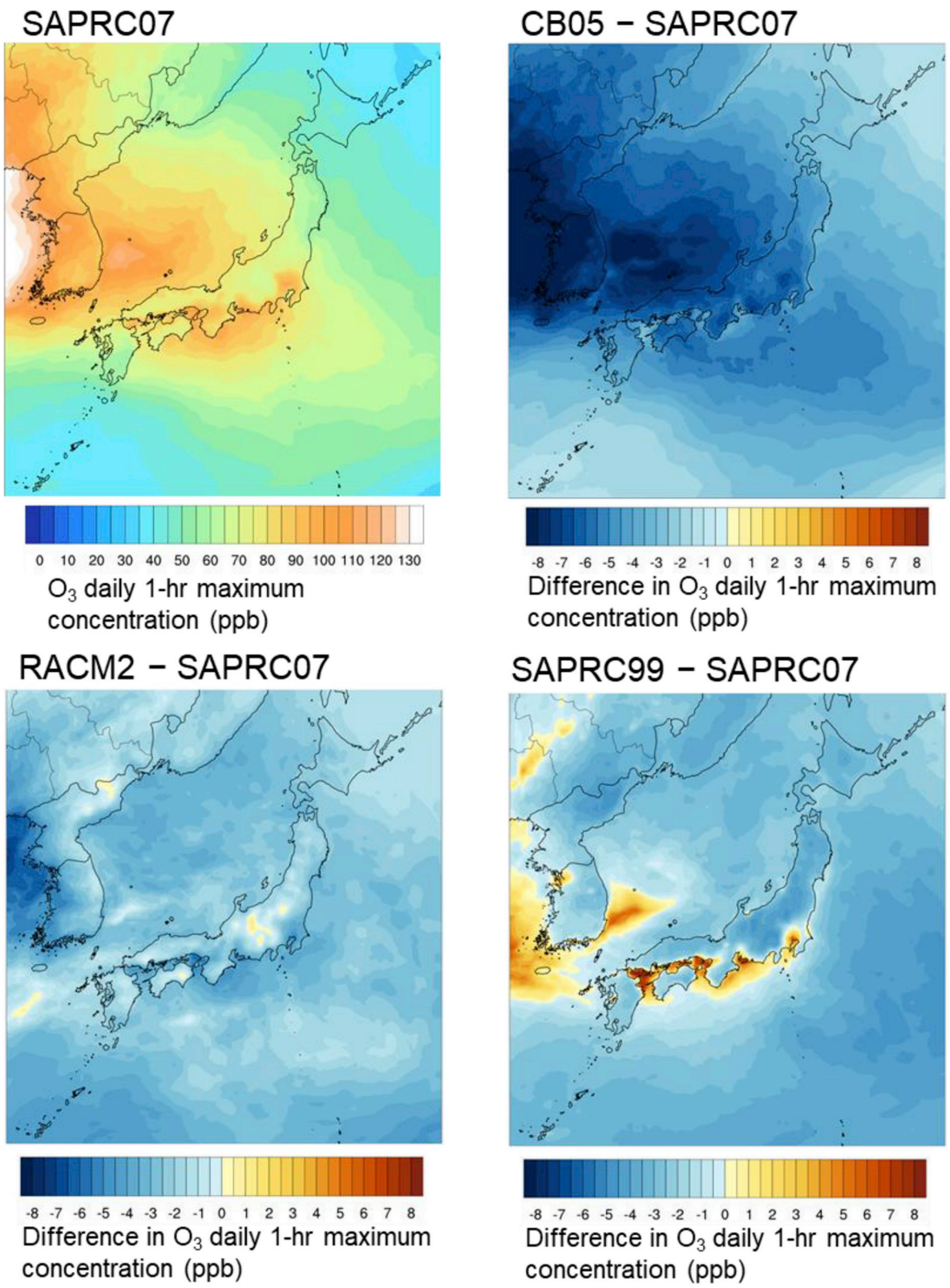

Fig. 5. Distributions of daily 1 h maximum O_3 concentrations averaged over the target season and differences between the concentrations produced by the chemical mechanisms, shown over d02.

3. Results and discussion

3.1. O_3 concentration distributions

O_3 concentration distributions during the study period are discussed below for the given domains. The SAPRC07TC average daily 1 h maximum O_3 concentration distribution during the study period for d01 and d02 are shown in Figs. 4 and 5, respectively. The concentration distributions for the other chemical mechanisms are shown in terms of difference from the SAPRC07TC concentrations. In d01, the seasonal O_3

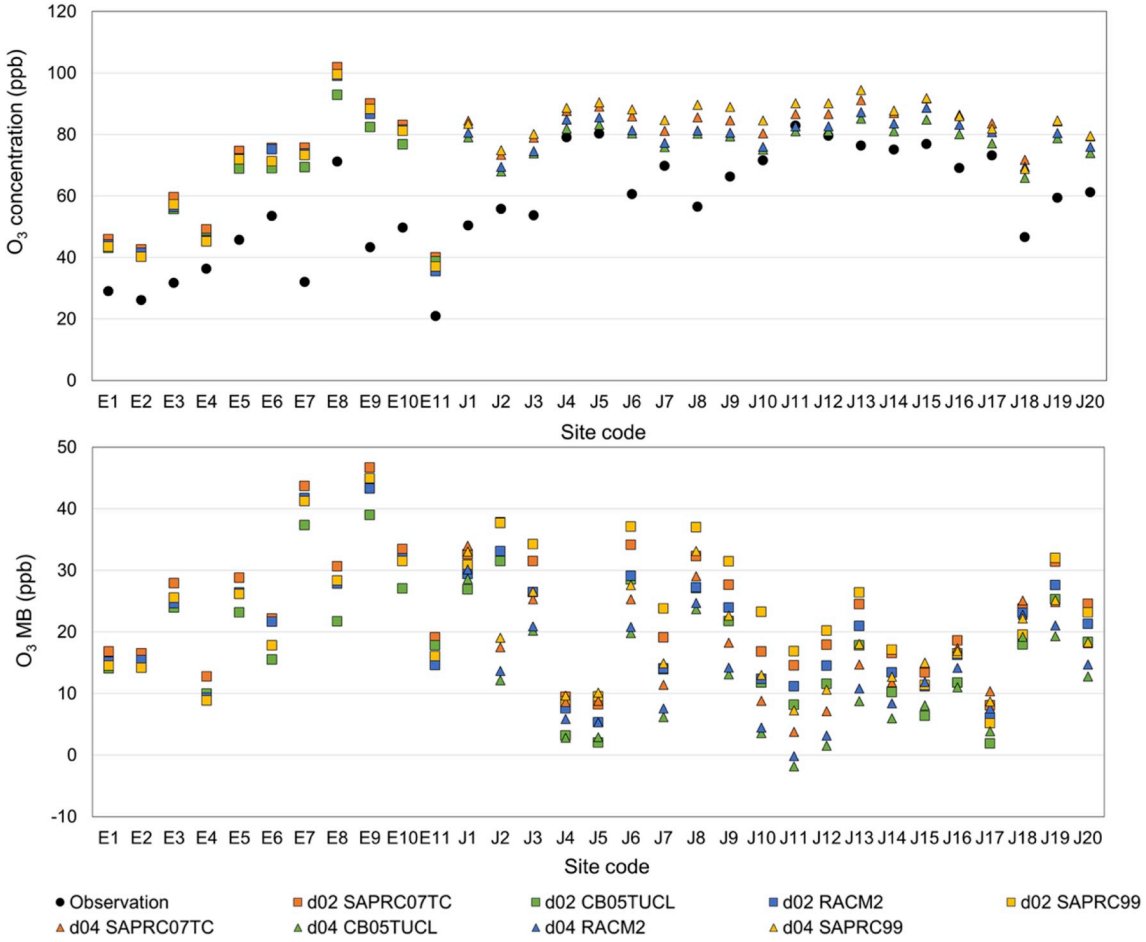

Fig. 6. Average and mean bias of the daily 1 h maximum O_3 concentrations for the chemical mechanisms during the study period at the observation sites. Site codes are shown in Fig. 3. Squares and triangles are concentrations of d02 and d04, respectively.

concentration was high in Eastern China, where the emissions of O_3 precursors NO_x and CO were large (Kurokawa et al., 2013). This high concentration spread from Eastern China to Japan. In d02, high O_3 concentrations prevailed from the west. Areas with high concentrations of ~100 ppb were also confirmed in the urban areas in d04.

The O_3 concentration differences between CB05TUCL and SAPRC07TC were negative in the SAPRC07TC high O_3–concentration areas for both d01 and d02 (Figs. 4 and 5). The difference appears to be larger in the high O_3–concentration area for SAPRC07TC. The distribution of the difference suggests that the SAPRC07TC O_3 concentration was higher than that of CB05TUCL in most locations and under most conditions. The concentration differences between RACM2 and SAPRC07TC were negative in Eastern China and positive in the western part of d01. The differences were smaller in scale than those between CB05TUCL and SAPRC07TC. Furthermore, the differences were smaller in d02 than in d01. For SAPRC99, in contrast to CB05TUCL and RACM2, the differences were positive along the East China coast, off shore, and in Japanese cities but negative in the other areas in d01. The differences in d02 were also positive over urban areas and their offshore areas as well as the western area of the domain over the sea but negative in other areas. For all the chemical mechanisms, the average daily 1 h maximum O_3 concentration during the summer differed from that in SAPRC07TC by ± 10 ppb. The concentration differences between SAPRC99 and SAPRC07TC were consistent with the results of Cai et al. (2011), in which the SAPRC07 concentration was less than 10 ppb lower than that of SAPRC99 in high O_3–concentration areas in California. Sarwar et al. (2013) showed that the RACM2 O_3 concentration was less than 10% greater than that of CB05TUCL in the USA. Yu et al. (2010) showed that the normalized mean bias of O_3 for SAPRC99 was about 10% greater than that for CB05. Differences of the same magnitude are confirmed in Figs. 4 and 5; thus, the concentration differences between the chemical mechanisms in this study are similar to those found for the USA.

3.2. Comparison of modeled and observed concentrations

The O_3 concentrations produced by the chemical mechanisms were compared to those from observations from EANET and automatic monitoring sites (Fig. 6). The study period average daily 1 h maximum was used in the validation to focus on model uncertainty for high concentrations. The average concentrations produced by the four chemical mechanisms varied within ± 10 ppb at EANET and the automatic monitoring sites. CB05TUCL produced the lowest concentrations at all of the sites. The RACM2 concentrations were higher than those from CB05TUCL and lower than those from SAPRC07TC. The SAPRC99 concentrations were lower than those from SAPRC07TC for the EANET sites and higher than those from SAPRC07TC for most of the automatic monitoring sites. The SAPRC99 concentrations tended to be higher than those from the other mechanisms in urban areas. However, the concentration differences between the other chemical mechanisms were consistent for the monitoring sites.

To evaluate the O_3 concentration uncertainty for the chemical mechanisms, the bias distribution and differences between modeled and observed values were calculated for the daily 1 h maximum O_3 concentrations (Fig. 7). The differences in O_3 concentration between the chemical mechanisms were also calculated. The mean bias (MB) values

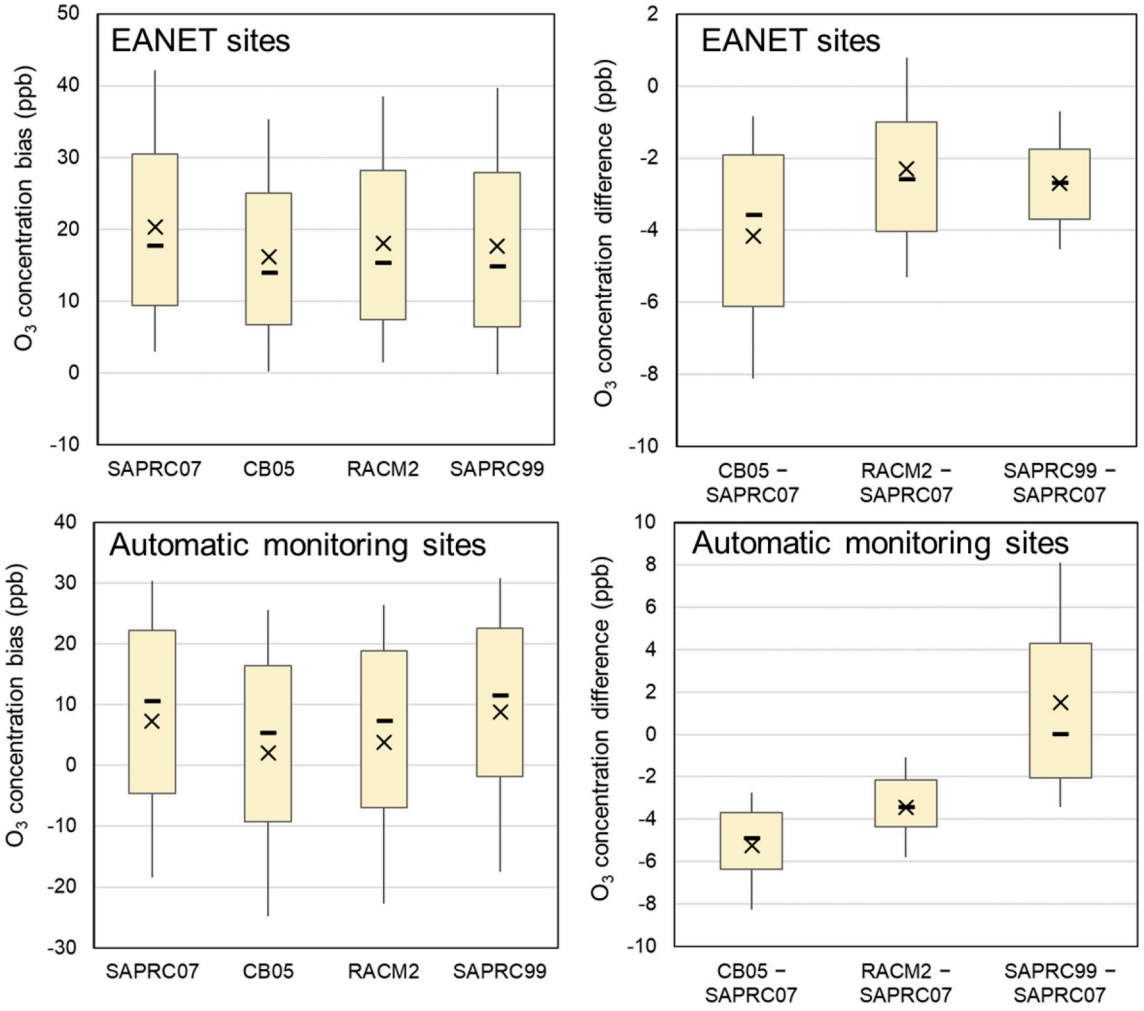

Fig. 7. Distributions of bias for the four chemical mechanisms as well as O_3 concentration differences between SAPRC07TC and the other mechanisms for EANET and automatic monitoring sites. The top of the bar, top of the box, bottom of the box, and bottom of the bar indicate the 90th, 75th, 25th, and 10th percentiles, respectively. Horizontal bars indicate the median, and cross markers denote the mean.

for the automatic monitoring sites were relatively low compared to those for the EANET sites. The O_3 concentration MB tended to be lower for the automatic monitoring sites than for the EANET sites. The difference between the d02 and d04 grid resolutions was a factor in the MB differences between the sites. To evaluate these MB differences due to grid size, the MB was calculated for sites J1–J20 using the result from the d02 grids; the resultant MB values ranged from −12 to 42 ppb with an average of 14 ppb. The grid resolution influenced the MB, but the MB varied between the sites. The difference in MB between EANET and automatic monitoring sites may also have been influenced by the site locations, which were in rural and urban areas, respectively. The bias produced by the four chemical mechanisms ranged from 0 to 42 ppb with an average of 18 ppb for the EANET sites and from −25 to 31 ppb with an average of 5.5 ppb for the automatic monitoring sites. The simulated O_3 concentration was overestimated at most sites. Furthermore, the differences in concentration between the chemical mechanisms ranged from −8 to 1 ppb with an average of −3.1 ppb for the EANET sites and from −8 to 8 ppb with an average of −2.4 ppb for the automatic monitoring sites. The model bias was much larger than the differences in concentration between the chemical mechanisms. Therefore, the model overestimation was not explained by the differences between the chemical mechanisms.

3.3. Process analysis for O_3 concentrations in the domains

Process analysis was conducted for the O_3 concentration IPRs to clarify the causes of the uncertainties in the chemical mechanisms using the chemical process rates. During the analysis, the hourly IPRs in the daytime (5–19) were averaged in d02 and d04 from the 1st to the 10th vertical layers over the study period (Fig. 8). The daily 1 h maximum average of chemical IPR for O_3 over the land and sea areas of d02 and d04 are also shown in Fig. 9 for the comparison with daily 1-h maximum O_3 concentration. In the domains, the IPRs were divided into land and sea areas using land use data from the Weather Research and Forecasting Model. The IPRs of the chemical process were larger than those of the other processes, except for the sea area of d02. The low IPRs of the chemical process over the sea area of d02 were derived from the low O_3 concentration compared to that over the land area as shown in Fig. 5. The average of the chemical IPR over the land area of d04 was approximately 1 ppb h^{-1} and was 0.5 ppb h^{-1} in both the land area of d02 and the sea area of d04. Over the land area, the daily 1 h maximum average of the chemical IPR showed the same trend as the O_3 concentration. Over the sea area, the daily 1-h maximum average of the chemical IPR for SAPRC99 was high and that for RACM2 was low in the chemical mechanisms. This trend is also shown for the O_3 concentration in Fig. 5. For the other processes, the advection and diffusion IPRs were positive in d02 and negative in d04. These values were affected by lower O_3 concentration in d02 and higher O_3 concentration in d04,

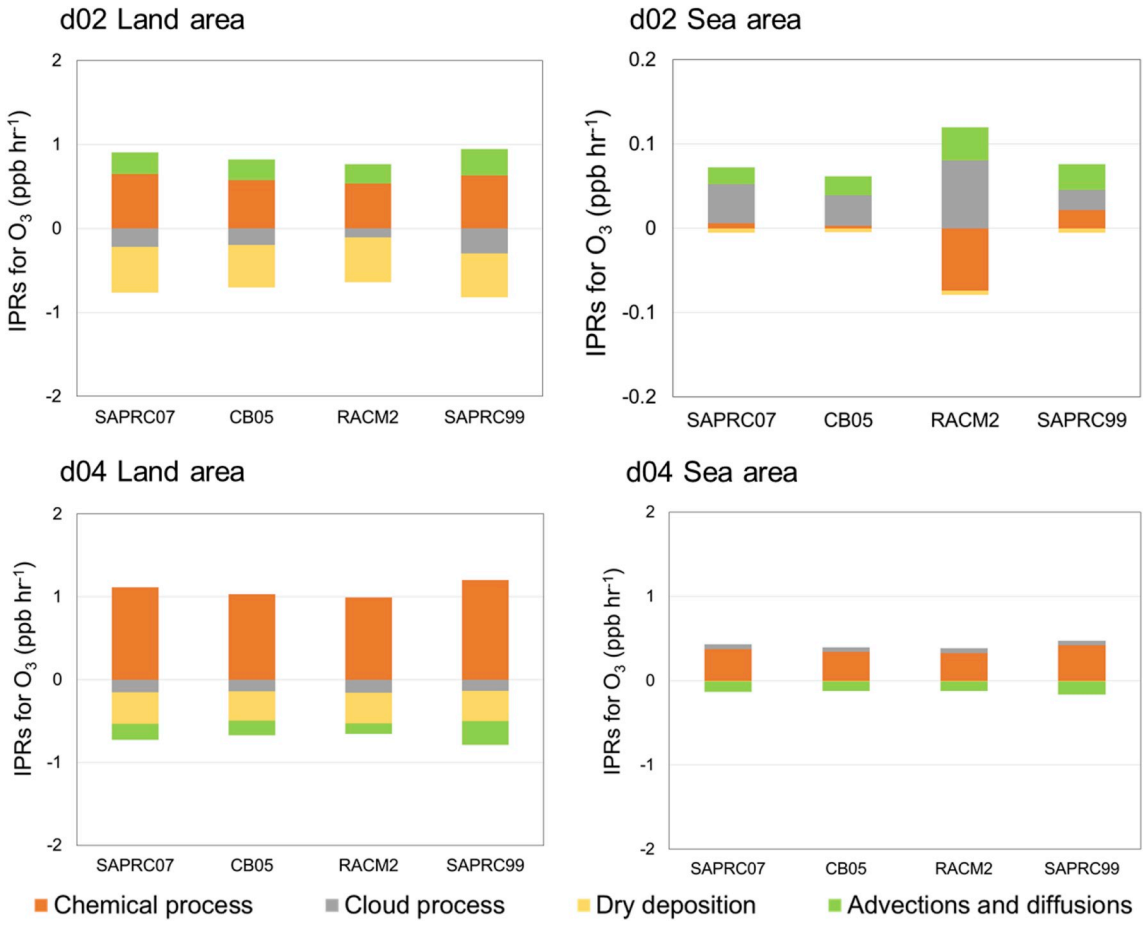

Fig. 8. Daytime averages of O_3 concentration integrated process rates (IPRs) in the given domains for the four chemical mechanisms. The IPRs were averaged in the daytime of the study period from the 1st to the 10th vertical layers over d02 and d04, which were divided into land and sea areas.

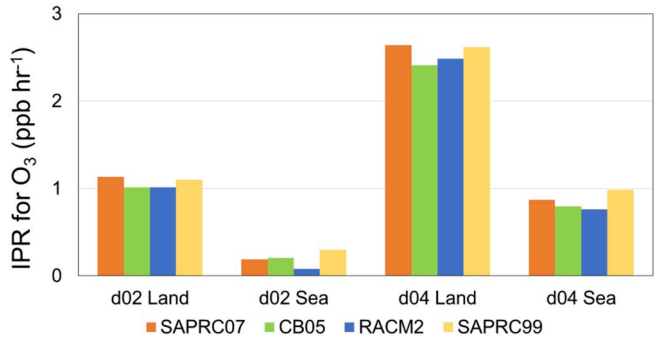

Fig. 9. Daily 1 h maximum averages of chemical O_3 integrated process rates (IPRs) in the given domains for the four chemical mechanisms. The IPRs were averaged from the 1st to the 10th vertical layers over d02 and d04, which were divided into land and sea areas.

compared to that in the outer area of the domain shown in Figs. 4 and 5. For dry deposition, negative IPRs were calculated in all cases, especially over land. The difference in IPR between land and sea may be explained by the lower deposition velocity for water surfaces (in comparison to other land uses; Byun and Ching, 1999). Cloud processes include vertical convective mixing of high O_3 concentrations in the upper to the target layers and wet deposition. Over the land areas of d02 and d04, the cloud process IPRs were negative due to wet deposition being higher than the convective mixing. In these areas, O_3 produced by high chemical IPR caused high wet deposition by scavenging. The IPR over the sea area of d02 was positive due to the convective mixing being larger than wet deposition. In this area, wet deposition was low because of the low chemical IPR.

The differences in the chemical IPRs between the chemical mechanisms showed the same trend as those of the daily 1 h maximum O_3 concentrations in Fig. 4, expect for RACM2. For the other three chemical mechanisms, IPRs ranked as follows over the land area of d02: SAPRC07TC > SAPRC99 > CB05TUCL; those in the other areas ranked as follows: SAPRC99 > SAPRC07TC > CB05TUCL. In contrast to the O_3 concentration case, the IPRs of the RACM2 chemical process was lower than that for CB05TUCL. The low negative IPRs of the other processes for RACM2 contributed to the higher O_3 concentration than that for CB05TUCL in all cases apart from the sea area of d02. In this area, the IPRs of the chemical process for RACM2 were negative, which differed from those for the other chemical mechanisms. The relatively high IPRs of the cloud, advection, and diffusions processes for RACM2 balanced the total IPRs in this case. The differences between the daytime chemical IPRs of the chemical mechanisms approximately corresponded to the difference in daily 1 h maximum O_3 concentrations.

Process analysis was also applied for the EANET and automatic monitoring sites. The IPRs were averaged from 1st to 10th layers in one grid, including one of the monitoring sites for the daytime of the target period (Fig. 10). The IPRs of the processes other than the chemical process were distributed inversely to the chemical process in the same way as the IPRs for the land area of d04 in Fig. 8. For the J2 and J10 sites, negative IPRs of the chemical process caused the lower O_3 concentrations compared with those in the surrounding sites. Positive IPRs of the advection and diffusions balanced the O_3 concentration changes in these sites. The distributions of the IPRs of the chemical mechanisms showed the same trend as d04's means in Fig. 8. The chemical process IPRs of the chemical mechanisms in the automatic monitoring sites

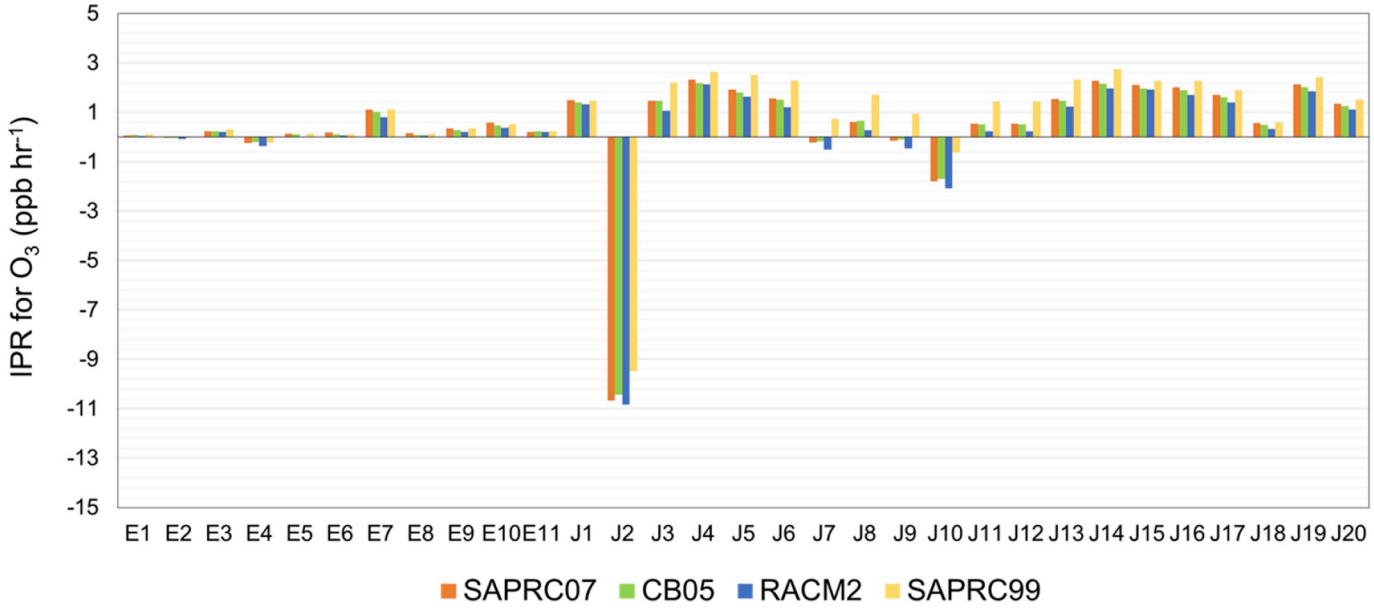

Fig. 10. Daytime averages of the chemical process integrated process rates (IPRs) for O_3 concentrations in the monitoring sites. The IPR is averaged from the 1st to the 10th vertical layers in a grid including the monitoring site over the daytime of the study period.

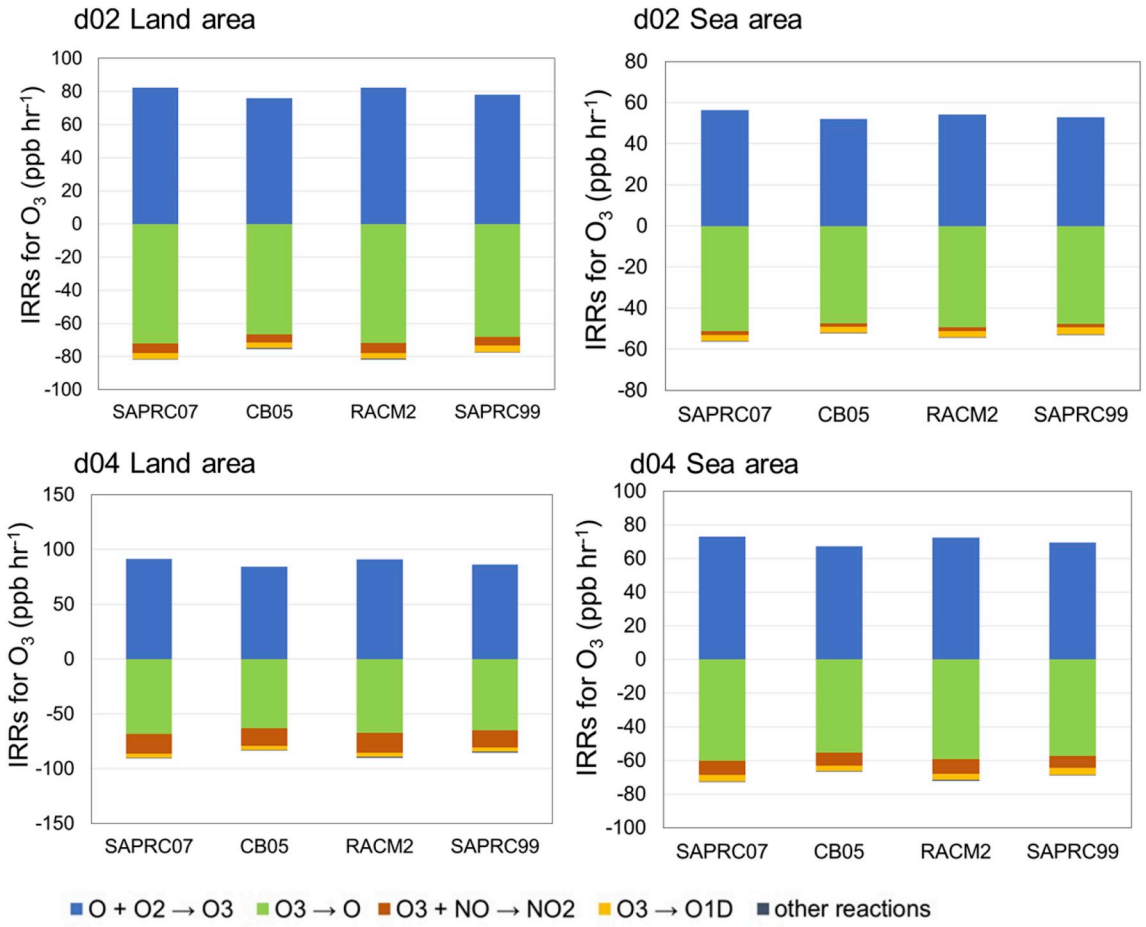

Fig. 11. Daytime averages of integrated reaction rates (IRRs) for reactions related to O_3 over the land and sea areas of the domains for the four chemical mechanisms. The integrated process rates were averaged over the daytime of the study period from the 1st to the 10th vertical layers over d02 and d04.

(J1–J20) were ranked as follows: SAPRC99 > SAPRC07TC > CB05TUCL > RACM2. For the EANET sites, the IPR of SAPRC99 was close to that of SAPRC07TC compared with IPRs of the automatic sites.

3.4. Reaction rates related to O_3 chemical processes

The IRRs for reactions related to O_3 concentration were calculated to find the reactions that influence the differences in O_3 concentration

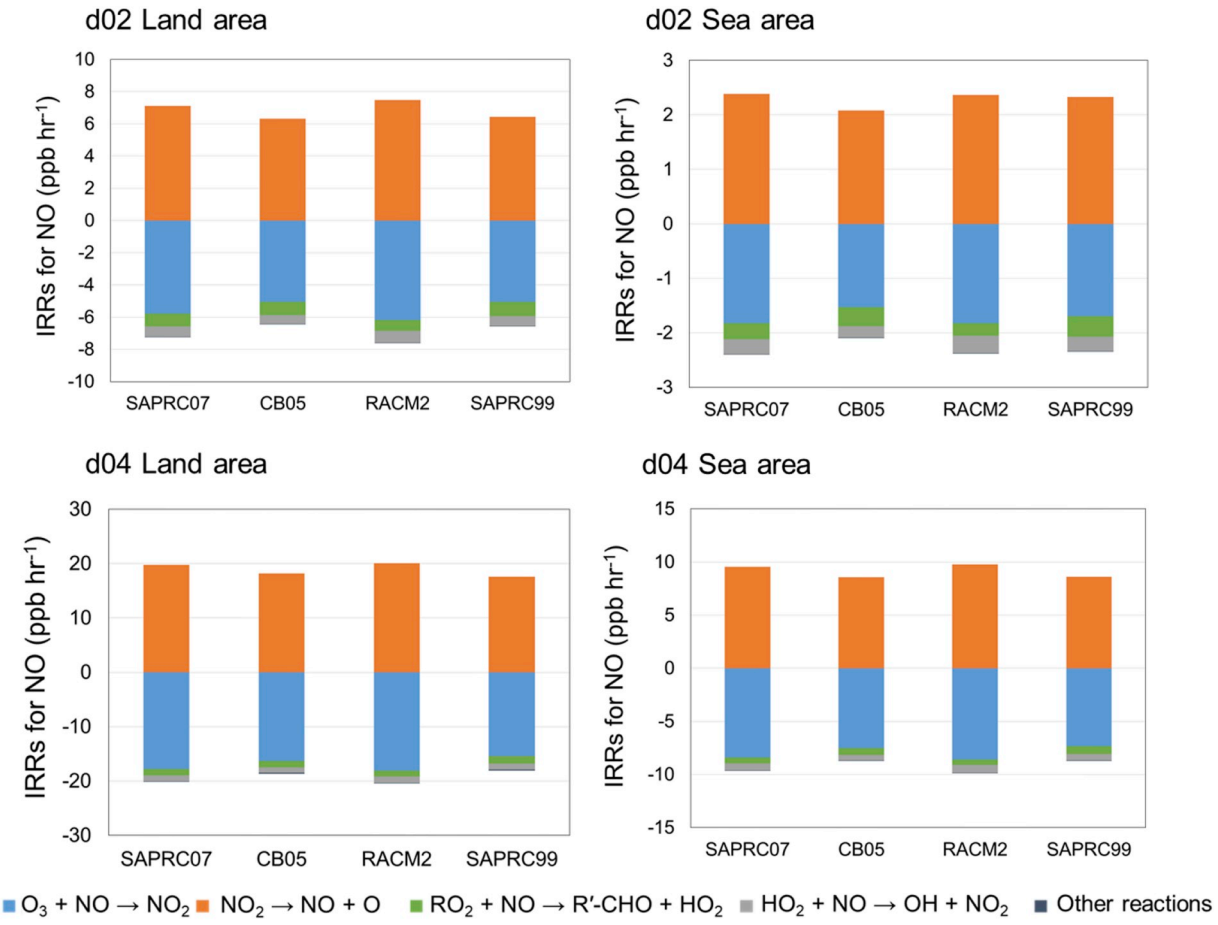

Fig. 12. Daytime averages of integrated reaction rates (IRRs) for reactions related to NO over the land and sea areas of the domains for the four chemical mechanisms. The integrated process rates were averaged over the daytime of the study period from the 1st to the 10th vertical layers over d02 and d04.

between the chemical mechanisms. Like the IPRs, the daytime (5–19) hourly IRRs were averaged over the target domain, layer, and period for the four mechanisms (Fig. 11). The major IRR for O_3 was found to be the reaction between O (^{3}P) and O_2. The second-largest absolute IRR was found in the reactions converting O_3 to O (^{3}P), and the next largest IRRs were the reactions between O_3 and NO and those converting O_3 to O (^{1}D). The IRRs of these reactions also contributed to the differences in O_3 concentration etween the chemical mechanisms. Considering that the differences in chemical process rates between the chemical mechanisms were within the range of – 0.1 to 0.1 ppb h^{-1} (Fig. 8), these four reactions could influence the O_3 concentration enough to cause the differences between the chemical mechanisms. The IRR of the reaction between O_3 and NO was influenced by reactions related to NO. The IRRs for reactions related to NO were calculated in a similar manner to the O_3 reaction IRRs to reveal the indirect influence of NO reactions on the O_3 concentration uncertainty in the chemical mechanisms (Fig. 12). Four reactions exerted a large influence on the differences in O_3 concentration between the chemical mechanisms.

To evaluate the relationships between these reactions and the O_3 concentration differences between the chemical mechanisms in detail, coefficients of determination (r^2) were calculated for the O_3 chemical IPR and IRR differences between the chemical mechanisms from SAPRC07TC (Table 2). Hourly daytime IPRs and IRRs averaged over the domains and layers 1–10 for both land and sea areas of d02 and d04 were used in the r^2 calculations. The highest r^2 between the IPR and IRR difference was found for the hydroperoxyl radical (HO_2)-NO reaction in CB05TUCL and SAPRC99 in all cases and the alkyl peroxyl radical (RO_2)-NO reaction in RACM2 in all cases except for the sea area of d04. These reactions consume NO to suppress the decrease in the O_3 concentration by the reaction between O_3 and NO. The high r^2 suggests that the difference in IRRs for these reactions of the chemical mechanisms largely contributed to the difference in the chemical process IPRs and O_3 concentration. Sadanaga et al. (2005) found the relationship by which instantaneous O_3 production was determined by NO reactions with HO_2 and RO_2. Chen et al. (2010) predicted the O_3 production of the different chemical mechanisms from predicted HO_2 and RO_2 concentrations. These reactions primarily influenced the O_3 concentration and the difference between the chemical mechanisms. Regarding the other reactions, the r^2 values for the O_3 reactions were relatively high for CB05TUCL. However, IRRs of these O_3 reactions could be affected by both O_3 concentration and reaction rate constants. The difference in O_3 concentration between SAPRC07TC and CB05TUCL could have caused the difference in IRRs between the O_3 reactions. The relation of IRRs to the O_3 reactions and chemical IPRs is discussed by comparing the reaction rate constants.

The IRR differences in the chemical mechanisms can be attributed to differences in the reactant and product concentrations and reaction rate constants. The influence of the differences in the reaction rate constants on the O_3 IPR difference was investigated by comparing the rate constants of the four chemical mechanisms (Table 3). The HO_2-NO reaction rate constant in CB05TUCL, RACM2, and SAPRC99 was lower than that in SAPRC07TC. This difference in the constant would influence the differences in IRRs. The reaction schemes and chemical compounds included in RO_2 differed between RACM2 and SAPRC07TC. The reaction rate constants for the reactions of MEO_2 and MEO_3 with NO were the same in all the chemical mechanisms. However, the rate constants were low compared with SAPRC07TC when the RO_2 carbon number in the reaction increased. The differences in rate constants and

Table 2
Coefficients of determination (r^2) of the daytime hourly O_3 integrated process rates (IPR) difference from SAPRC07TC and the corresponding integrated reaction rates (IRR) difference over the land and sea areas of d02 and d04.

d02	r^2 between O_3 chemical IPR and IRR differences from SAPRC07					
	Land area			Sea area		
	CB05	RACM2	SAPRC99	CB05	RACM2	SAPRC99
O_3 reactions corresponding to IRRs						
$O + O_2 \rightarrow O_3$	0.70	0.04	0.27	0.35	0.27	0.15
$O_3 + NO \rightarrow NO_2$	0.75	0.05	0.54	0.51	0.00	0.64
$O_3 \rightarrow O^1D$	0.90	0.10	0.73	0.59	0.18	0.55
$O_3 \rightarrow O$	0.64	0.07	0.18	0.29	0.22	0.11
NO reactions corresponding to IRRs						
$NO_2 \rightarrow NO + O$	0.81	0.02	0.66	0.59	0.01	0.80
$HO_2 + NO \rightarrow OH + NO_2$	0.90	0.05	0.89	0.68	0.07	0.89
$RO_2 + NO \rightarrow RO + NO_2$	0.02	0.90	0.00	0.16	0.88	< 0.01
d04	r^2 between O_3 chemical IPR and IRR differences from SAPRC07					
	Land area			Sea area		
	CB05	RACM2	SAPRC99	CB05	RACM2	SAPRC99
O_3 reactions corresponding to IRRs						
$O + O_2 \rightarrow O_3$	0.76	< 0.01	0.04	0.53	0.21	0.04
$O_3 + NO \rightarrow NO_2$	0.80	< 0.01	0.06	0.56	0.52	0.04
$O_3 \rightarrow O^1D$	0.82	0.01	0.30	0.64	0.02	0.35
$O_3 \rightarrow O$	0.67	0.01	0.01	0.45	< 0.01	0.03
NO reactions corresponding to IRRs						
$NO_2 \rightarrow NO + O$	0.82	0.01	0.09	0.61	0.59	0.07
$HO_2 + NO \rightarrow OH + NO_2$	0.92	0.09	0.80	0.77	0.43	0.74
$RO_2 + NO \rightarrow RO + NO_2$	0.20	0.77	< 0.01	0.25	0.48	0.01

Table 3
Reaction rate constants in the four chemical mechanisms for 1 mol cm^{-3} s^{-1} of the reactants at 1 atm and 298 K.

Reaction	CB05	SAPRC07	RACM2	SAPRC99
$O + O_2 \rightarrow O_3$	6.1×10^{-34}	5.8×10^{-34}	5.8×10^{-34}	5.8×10^{-34}
$O_3 + NO \rightarrow NO_2$	2.0×10^{-14}	2.0×10^{-14}	1.7×10^{-14}	1.8×10^{-14}
$O_3 \rightarrow O\ (^1D)$	photolysis	photolysis	photolysis	Photolysis
$O_3 \rightarrow O$	photolysis	photolysis	photolysis	Photolysis
$NO_2 \rightarrow NO + O$	photolysis	photolysis	photolysis	Photolysis
$HO_2 + NO \rightarrow OH + NO_2$	8.1×10^{-12}	8.9×10^{-12}	8.5×10^{-12}	8.4×10^{-12}
MEO_2[a] + NO → FORM[b] + HO_2 + NO_2	7.7×10^{-12}	7.7×10^{-12}	7.7×10^{-12}	7.3×10^{-12}
$MECO_3$[c] + NO → MEO_2 + CO_2 + NO_2	2.0×10^{-11}	2.0×10^{-11}	2.0×10^{-11}	2.1×10^{-11}
RO_2C[d] + NO → NO_2	–	9.3×10^{-12}	–	–
ETHP[e] + NO → HO_2 + NO_2	–	–	8.8×10^{-12}	–
HC3P[f] + NO → HO_2 + NO_2	–	–	4.0×10^{-12}	–
RO_2_R[g] + NO → NO_2 + HO_2	–	–	–	9.0×10^{-12}

[a] Methyl peroxy radicals.
[b] Formaldehyde.
[c] Acetyl peroxy radicals.
[d] Peroxy radical operator representing NO to NO_2 and NO_3 to NO_2 conversions and the effects of peroxy radical reactions on other species.
[e] Peroxy radicals formed from ethane.
[f] Peroxy radicals formed from propane.
[g] Peroxy radical operator representing NO to NO_2 conversion with HO_2 formation.

lumped chemical compounds in the reaction could have influenced the IRR difference between RACM2 and SAPRC07TC. The lower IRR of the RO_2-NO reaction for RACM2 compared to that for the other mechanisms is also shown in Figs. 8 and 9 in terms of the low O_3 chemical IPR over the sea area. In d02, the ratio of averaged VOC to NO_x concentration was 3.7 over the land and 22.7 over the sea for RACM2. In d04, this ratio was 5.5 for the land and 8.4 for the sea. For the other mechanisms, the ratio was also high for the sea area, whereas the values varied because of different VOC emissions. Over the sea area, the high VOC concentration compared to the NO_x concentration was considered to increase the differences in IRRs for the RO_2-NO reaction and chemical IPRs for O_3 between RACM2 and the other mechanisms. For the O_3 reactions, the rate constants for the reaction of O and O_2 producing O_3 were large for CB05TUCL and similar for the other mechanisms. The rate constants for the reaction between O_3 and NO were the same for SAPRC07TC and CB05TUCL and low for RACM2 and SAPRC99. These values suggest that the O_3 concentrations of SAPRC07TC and CB05TUCL caused the IRR differences in the O_3 reactions in the mechanisms. Relatively high r^2 values for the O_3 reactions in Table 2 were considered to be due to this relation.

The IRRs of the reactions related to O_3 and NO_x for the EANET and automatic monitoring sites were calculated to focus on the difference in

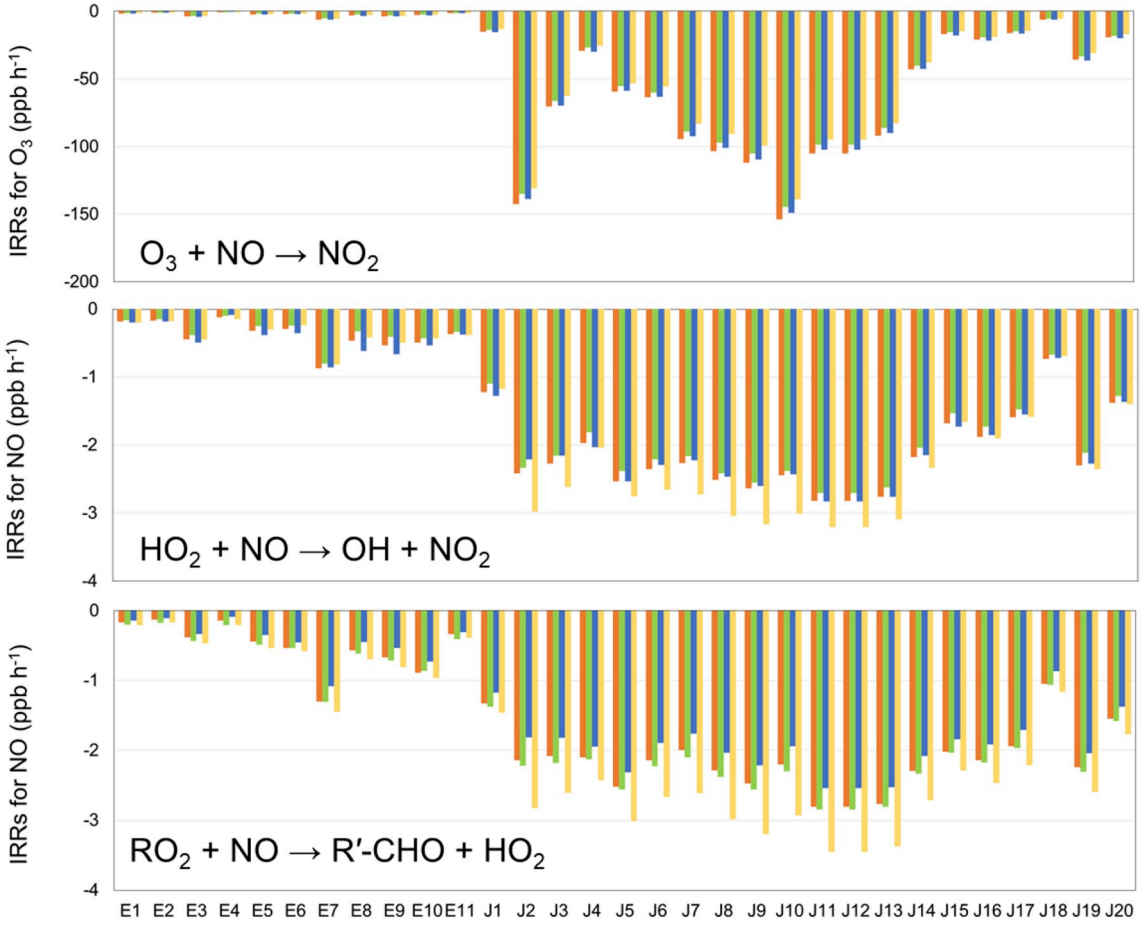

Fig. 13. Daytime averages of integrated reaction rates (IRRs) of the reactions, $O_3 + NO \rightarrow NO_2$, $HO_2 + NO \rightarrow OH + NO_2$, and $RO_2 + NO \rightarrow R'\text{-}CHO + HO_2$, for the EANET and automatic monitoring sites. The IRRs are averaged from the 1st to the 10th vertical layers in a grid including the monitoring site over the daytime of the study period.

the reaction rates between the chemical mechanisms in urban and rural sites. The IRRs were averaged from the 1st to 10th vertical layers in a grid including the monitoring sites over the daytime during the study period. Considering the relation of the O_3 concentration difference in the above discussion, the IRRs of the three reactions, namely $O_3 + NO \rightarrow NO_2$, $HO_2 + NO \rightarrow OH + NO_2$, and $RO_2 + NO \rightarrow R'\text{-}CHO + HO_2$, are shown in Fig. 13. The absolute IRRs of these reactions for the automatic monitoring sites were larger than those for the EANET sites. These reactions are related to NO_x and VOC. The difference in the IRRs between the sites was due to the concentrations and emissions of these gasses. This difference was clearer than those of the domain mean. The IRRs of the chemical mechanisms were distributed similarly to the domain mean except for one point. The absolute IRRs of SAPRC99 for the reaction between NO and HO_2 were relatively large in the urban area compared to those of the other chemical mechanisms. The absolute IRRs of SAPRC99 for the reaction between NO and RO_2 were also high in the EANET and automatic monitoring sites. These high absolute IRRs would contribute the large O_3 concentration of SAPRC99 in urban areas compared with those of the other chemical mechanisms. Considering the high correlation between the differences in the chemical O_3 IPRs and IRRs from SAPRC07TC in Table 2, the NO and HO_2 reaction contributed more to the difference in the O_3 concentrations of the chemical mechanisms than the NO and RO_2 reaction did. These high absolute IRRs of SAPRC99 in urban areas were due to relatively large emissions weighted to reacted OH rather than the reaction rate constants of these reactions, considering Fig. 2 and Table 3. The relatively low absolute IRRs in the NO reactions with HO_2 for CB05TUCL and RO_2 for RACM2 were consistent with the high correlations between the chemical IPR and IRR differences from SAPRC07TC in Table 2.

4. Conclusions

O_3 concentrations from four chemical mechanisms, namely CB05TUCL, RACM2, SAPRC07TC, and SAPRC99, were simulated by the CMAQ model for the Japanese region, and the O_3 concentration uncertainty was evaluated. The CB05TUCL mechanism produced the lowest O_3 concentrations over the entire target region. The second- and third-lowest O_3 concentrations were produced by RACM2 and SAPRC99, respectively. Over most of the target domain, SAPRC07TC produced the highest O_3 concentrations, though the concentrations from SAPRC99 exceeded those from SAPRC07TC in some areas. The concentration differences between the chemical mechanisms were between −10 and 10 ppb from the SAPRC07TC concentration, which was used as a standard. The biases between the modeled O_3 concentration and observations from monitoring sites were within 40 ppb, but the model largely overestimated the concentration. The uncertainty in the chemical mechanisms regarding O_3 concentration was much lower than the model bias. The chemical model uncertainty accounted for a part of the overall model uncertainty. However, the majority of the model uncertainty could be attributed to other factors, such as emissions, meteorological inputs, transport, and deposition. The over-estimation of the MEGAN biogenic VOC emissions reported by Carlton and Baker (2011), Hogrefe et al. (2011), and Chatani et al. (2018a) is potentially one of these factors. In recent studies, boundary conditions were found to affect O_3 concentrations (Hogrefe et al., 2018). Additionally, newer chemical mechanisms include halogen chemistry, which can reduce O_3

concentrations (Gantt et al., 2017). The influence of these potential factors on O_3 concentrations uncertainties will be investigated in future studies.

Factors influencing uncertainty in the chemical mechanisms were investigated through the IPRs and IRRs of O_3 and related species, which were calculated using process analysis. The domain- and 10-layer average of the O_3 IPR showed that the O_3 production process rates in SAPRC07TC were higher than those in the CB05TUCL and RACM2, especially over land. For SAPRC99, the O_3 production IPRs were larger than those from SAPRC07TC in d04 and over the sea in d02. The IRR analysis indicated that the differences in the O_3 chemical IPRs could have been caused by three O_3 production and loss reactions and related NO reactions. The coefficients of determination between the O_3 IPR and IRR differences showed the strongest correlation in IRR differences for the HO_2-NO reaction in CB05TUCL and SAPRC99 and the RO_2-NO reaction in RACM2. Differences in reaction rate constants and lumped VOCs may have caused some of the differences in O_3 production between the chemical models.

Acknowledgments

This research was supported by the Environment Research and Technology Development Fund (5-1601) of the Environmental Restoration and Conservation Agency. The JATOP emissions inventory database was provided by the Japan Petroleum Energy Center. The ship emissions around Japan were produced by the Sasakawa Peace Foundation (formerly the Ocean Policy Research Foundation) through a project evaluating air quality improvements due to emissions control areas. The authors appreciate the cooperation of the J-STREAM participants.

Appendix A. Supplementary data

Supplementary data to this article can be found online at https://doi.org/10.1016/j.atmosenv.2018.11.003.

References

Byun, D.W., Ching, J.K.S., 1999. Science Algorithms of the EPA Models-3 Community Multiscale Air Quality (CMAQ) Modeling System. EPA/600/R-99/030 (NTIS PB2000-100561). US Environ. Prot. Agency, Off. Res. Dev., Washington, DC, USA.

Byun, D.W., Schere, K.L., 2006. Review of the governing equations, computational algorithms, and other components of the Models-3 Community Multiscale Air Quality (CMAQ) modeling system. Appl. Mech. Rev. 59, 51–77. https://doi.org/10.1115/1.2128636.

Cai, C., Kelly, J.T., Avise, J.C., Kaduwela, A.P., Stockwell, W.R., 2011. Photochemical modeling in California with two chemical mechanisms: model intercomparison and response to emission reductions. J. Air Waste Manag. Assoc. 61, 559–572. https://doi.org/10.3155/1047-3289.61.5.559.

Carter, W.P.L., 2000. Implementation of the SAPRC-99 Chemical Mechanism into the Models-3 Framework. Report to the United States Environmental Protection Agency. Available online. http://www.engr.ucr.edu/~carter/pubs/s99mod3.pdf, Accessed date: 11 December 2017.

Carter, W.P.L., 2010a. Development of the SAPRC-07 chemical mechanism. Atmos. Environ. 44, 5324–5335. https://doi.org/10.1016/j.atmosenv.2010.01.026.

Carter, W.P.L., 2010b. Development of a condensed SAPRC-07 chemical mechanism. Atmos. Environ. 44, 5336–5345. https://doi.org/10.1016/j.atmosenv.2010.01.024.

Carter, W.P.L., 2016. Spreadsheet with speciation assignments and macros to output files for speciation processing by SMOKE and the Speciation Tool. Available online. http://www.engr.ucr.edu/~carter/emitdb/SpecDB.xls, Accessed date: 20 December 2017.

Carter, R., Atkinson, W.P.L., 1996. Development and evaluation of a detailed mechanism for the atmospheric reactions of isoprene and NO_x. Int. J. Chem. Kinet. 28 497e530.

Carter, W.P.L., Luo, D., Malkina, I.L., 2000. Investigation of Atmospheric Reactivities of Selected Consumer Product VOCs. Final Report to California Air Resources Board Contract 95-308. Coll. Eng., Center Environ. Res. Tech., Univ. Calif., Riverside, CA, USA.

Carlton, A.G., Baker, K.R., 2011. Photochemical modeling of the ozark isoprene volcano: MEGAN, BEIS, and their impacts on air quality predictions. Environ. Sci. Technol. 45, 4438–4445.

Chatani, S., Matsunaga, S.N., Nakatsuka, S., 2015. Estimate of biogenic VOC emissions in Japan and their effects on photochemical formation of ambient ozone and secondary organic aerosol. Atmos. Environ. 120, 38–50. https://doi.org/10.1016/j.atmosenv.2015.08.086.

Chatani, S., Morikawa, T., Nakatsuka, S., Matsunaga, S., Minoura, H., 2011. Development of a framework for a high-resolution, three-dimensional regional air quality simulation and its application to predicting future air quality over Japan. Atmos. Environ. 45, 1383–1393. https://doi.org/10.1016/j.atmosenv.2010.12.036.

Chatani, S., Okumura, M., Shimadera, H., Yamaji, K., Kitayama, K., Matsunaga, S.N., 2018a. Effects of a detailed vegetation database on simulated meteorological fields, biogenic VOC emissions, and ambient pollutant concentrations over Japan. Atmosphere 9, 179. https://doi.org/10.3390/atmos9050179.

Chatani, S., Yamaji, K., Sakurai, T., Itahashi, S., Shimadera, H., Kitayama, K., Hayami, H., 2018b. Overview of model inter-comparison in Japan's study for reference air quality modeling (J-STREAM). Atmosphere 9, 19. https://doi.org/10.3390/atmos9010019.

Chen, S., Ren, X., Mao, J., Chen, Z., Brune, W.H., Lefer, B., Rappenglück, B., Flynn, J., Olson, J., Crawford, J.H., 2010. A comparison of chemical mechanisms based on TRAMP-2006 field data. Atmos. Environ. 44, 4116–4125. https://doi.org/10.1016/j.atmosenv.2009.05.027.

Diehl, T., Heil, A., Chin, M., Pan, X., Streets, D., Schultz, M., Kinne, S., 2012. Anthropogenic, biomass burning, and volcanic emissions of black carbon, organic carbon, and SO_2 from 1980 to 2010 for hindcast model experiments. Atmos. Chem. Phys. Discuss. 12, 24895–24954. https://doi.org/10.5194/acpd-12-24895-2012.

EANET (Acid Deposition Monitoring Network in East Asia), 2014. Data Report 2013. Asia Center for Air Poll. Res, Niigata-shi, Japan.

Gantt, B., Sarwar, G., Xing, J., Simon, H., Schwede, D., Hutzell, W.T., Mathur, R., Saiz-Lopez, A., 2017. The impact of iodide-mediated ozone deposition and halogen chemistry on surface ozone concentrations across the continental United States. Environ. Sci. Technol. 51, 1458–1466. https://doi.org/10.1021/acs.est.6b03556.

Gemmill, W., Katz, B., Li, X., 2007. The daily real-time, global Sea Surface temperature-high resolution analysis: RTG_SST_HR. Environ. Mod. Center Nat. Weather Serv. 260, 1–22 (Camp Springs, MD, USA).

Gipson, G.L., 1999. Process analysis. In: Byun, D.W., Ching, J.K.S. (Eds.), Science Algorithms of the EPA Models-3 Community Multiscale Air Quality (CMAQ) Modeling System. US Environ. Prot. Agency, Washington DC, USA 16-1–16-20. EPA/600/R-99/030 (NTIS PB2000-100561).

Goliff, W.S., Stockwell, W.R., Lawson, C.V., 2013. The regional atmospheric chemistry mechanism, version 2. Atmos. Environ. 68, 174–185. https://doi.org/10.1016/j.atmosenv.2012.11.038.

Guenther, A.B., Jiang, X., Heald, C.L., Sakulyanontvittaya, T., Duhl, T., Emmons, L.K., Wang, X., 2012. The model of emissions of gases and aerosols from Nature version 2.1 (MEGAN2.1): an extended and updated framework for modeling biogenic emissions. Geosci. Model Dev. 5, 1471–1492. https://doi.org/10.5194/gmd-5-1471-2012.

Hogrefe, C., Isukapalli, S.S., Tang, X., Georgopoulos, P.G., He, S., Zalewsky, E.E., Hao, W., Ku, J.-Y., Key, T., Sistla, G., 2011. Impact of biogenic emission uncertainties on the simulated response of ozone and fine particulate matter to anthropogenic emission reductions. J. Air Waste Manag. Assoc. 61, 92–108.

Hogrefe, C., Liu, P., Pouliot, G., Mathur, R., Roselle, S., Flemming, J., Lin, M., Park, R.J., 2018. Impacts of different characterizations of large-scale background on simulated regional-scale ozone over the continental United States. Atmos. Chem. Phys. 18, 3839–3864.

Huang, M., Carmichael, G.R., Bradley Pierce, R., Jo, D.S., Park, R.J., Flemming, J., Emmons, L.K., Bowman, K.W., Henze, D.K., Davila, Y., Sudo, K., Jonson, J.E., Tronstad Lund, M., Janssens-Maenhout, G., Dentener, F.J., Keating, T.J., Oetjen, H., Payne, V.H., 2017. Impact of intercontinental pollution transport on North American ozone air pollution: an HTAP phase 2 multi-model study. Atmos. Chem. Phys. 17, 5721–5750. https://doi.org/10.5194/acp-17-5721-2017.

Janssens-Maenhout, G., Crippa, M., Guizzardi, D., Dentener, F., Muntean, M., Pouliot, G., Keating, T., Zhang, Q., Kurokawa, J., Wankmüller, R., Denier van der Gon, H., Kuenen, J.J.P., Klimont, Z., Frost, G., Darras, S., Koffi, B., Li, M., 2015. HTAP_v2.2: a mosaic of regional and global emission grid maps for 2008 and 2010 to study hemispheric transport of air pollution. Atmos. Chem. Phys. 15, 11411–11432. https://doi.org/10.5194/acp-15-11411-2015.

Japan Meteorological Agency, 2017. Reports on volcanic activities (In Japanese). Available online. http://www.data.jma.go.jp/svd/vois/data/tokyo/volcano.html, Accessed date: 27 October 2017.

Khiem, M., Ooka, R., Hayami, H., Yoshikado, H., Huang, H., Kawamoto, Y., 2010. Process analysis of ozone formation under different weather conditions over the Kanto region of Japan using the MM5/CMAQ modelling system. Atmos. Environ. 44, 4463–4473. https://doi.org/10.1016/j.atmosenv.2010.07.038.

Knote, C., Tuccella, P., Curci, G., Emmons, L., Orlando, J.J., Madronich, S., Baró, R., Jiménez-Guerrero, P., Luecken, D., Hogrefe, C., Forkel, R., Werhahn, J., Hirtl, M., Pérez, J.L., San José, R., Giordano, L., Brunner, D., Yahya, K., Zhang, Y., 2015. Influence of the choice of gas-phase mechanism on predictions of key gaseous pollutants during the AQMEII phase-2 intercomparison. Atmos. Environ. 115, 553–568. https://doi.org/10.1016/j.atmosenv.2014.11.066.

Kurokawa, J., Ohara, T., Morikawa, T., Hanayama, S., Janssens-Maenhout, G., Fukui, T., Kawashima, K., Akimoto, H., 2013. Emissions of air pollutants and greenhouse gases over Asian regions during 2000–2008: regional Emission inventory in ASia (REAS) version 2. Atmos. Chem. Phys. 13, 11019–11058. https://doi.org/10.5194/acp-13-11019-2013.

Li, L., Chen, C.H., Huang, C., Huang, H.Y., Zhang, G.F., Wang, Y.J., Wang, H.L., Lou, S.R., Qiao, L.P., Zhou, M., Chen, M.H., Chen, Y.R., Streets, D.G., Fu, J.S., Jang, C.J., 2012. Process analysis of regional ozone formation over the Yangtze River Delta, China using the Community Multi-scale Air Quality modelling system. Atmos. Chem. Phys. 12, 10971–10987. https://doi.org/10.5194/acp-12-10971-2012.

Liu, X.-H., Zhang, Y., Cheng, S.-H., Xing, J., Zhang, Q., Streets, D.G., Jang, C., Wang, W.-X., Hao, J.-M., 2010. Understanding of regional air pollution over China using CMAQ, part I performance evaluation and seasonal variation. Atmos. Environ. 44, 2415–2426. https://doi.org/10.1016/j.atmosenv.2010.03.035.

Morino, Y., Chatani, S., Hayami, H., Sasaki, K., Mori, Y., Morikawa, T., Ohara, T., Hasegawa, S., Kobayashi, S., 2010. Evaluation of ensemble approach for O_3 and $PM_{2.5}$ simulation. Asian J. Atmos. Environ. 4, 150–156. https://doi.org/10.5572/ajae.2010.4.3.150.

Nawahda, A., Yamashita, K., Ohara, T., Kurokawa, J., Ohizumi, T., Chen, F., Akimoto, H., 2013. Premature mortality in Japan due to ozone. Atmos. Environ. 81, 538–545. https://doi.org/10.1016/j.atmosenv.2013.09.049.

NCEP (National Centers for Environmental Prediction), 2000. NCEP FNL operational model global tropospheric analyses, continuing from July 1999. In: Res. Data Arch. Nat. Center Atmos. Res. Comput. Inform. Syst. Lab., Boulder, CO, USA.

Sadanaga, Y., Yoshino, A., Kato, S., Kajii, Y., 2005. Measurements of OH reactivity and photochemical ozone production in the urban atmosphere. Environ. Sci. Technol. 39, 8847–8852. https://doi.org/10.1021/es049457p.

Sarwar, G., Godowitch, J., Henderson, B.H., Fahey, K., Pouliot, G., Hutzell, W.T., Mathur, R., Kang, D., Goliff, W.S., Stockwell, W.R., 2013. A comparison of atmospheric composition using the carbon bond and regional atmospheric chemistry mechanisms. Atmos. Chem. Phys. 13, 9695–9712. https://doi.org/10.5194/acp-13-9695-2013.

Sarwar, G., Luecken, D., Yarwood, G., Whitten, G.Z., Carter, W.P.L., 2008. Impact of an updated Carbon Bond mechanism on predictions from the CMAQ modeling system: preliminary assessment. J. Appl. Meteorol. Climatol. 47, 3–14. https://doi.org/10.1175/2007JAMC1393.1.

Skamarock, W.C., Klemp, J.B., Dudhia, J., Gill, D.O., Barker, D.M., Wang, W., Powers, J.G., 2008. A description of the Advanced Research WRF version 3. Nat. Center Atmos. Res. 1–113 NCAR/TN-475 + STR, (Boulder, CO, USA).

Sudo, K., Takahashi, M., Kurokawa, J., Akimoto, H., 2002. CHASER: a global chemical model of the troposphere. 1. Model description. J. Geophys. Res. 107 ACH 7-1–ACH 7-20. https://doi.org/10.1029/2001JD001113.

Tang, H., Pang, J., Zhang, G., Takigawa, M., Liu, G., Zhu, J., Kobayashi, K., 2014. Mapping ozone risks for rice in China for years 2000 and 2020 with flux-based and exposure-based doses. Atmos. Environ. 86, 74–83. https://doi.org/10.1016/j.atmosenv.2013.11.078.

Trieu, T.T.N., Goto, D., Yashiro, H., Murata, R., Sudo, K., Tomita, H., Satoh, M., Nakajima, T., 2017. Evaluation of summertime surface ozone in Kanto area of Japan using a semi-regional model and observation. Atmos. Environ. 153, 163–181. https://doi.org/10.1016/j.atmosenv.2017.01.030.

US EPA (U.S. Environmental Protection Agency), 2006. Air Quality Criteria for Ozone and Related Photochemical Oxidants (Final). EPA/600/R-05/004aF-cF. U.S. Environ. Prot. Agency, Washington, DC, USA.

Van der Werf, G.R., Randerson, J.T., Giglio, L., Van Leeuwen, T.T., Chen, Y., Rogers, B.M., Mu, M., Van Marle, M.J.E., Morton, D.C., Collatz, G.J., Yokelson, R.J., Kasibhatla, P.S., 2017. Global fire emissions estimates during 1997–2016. Earth Syst. Sci. Data 9, 697–720. https://doi.org/10.5194/essd-9-697-2017.

Whitten, G.Z., Heo, G., Kimura, Y., McDonald-Buller, E., Allen, D.T., Carter, W.P.L., Yarwood, G., 2010. A new condensed toluene mechanism for Carbon Bond: CB05-TU. Atmos. Environ. 44, 5346–5355. https://doi.org/10.1016/j.atmosenv.2009.12.029.

Yamaguchi, M., Hoshino, D., Inada, H., Akhtar, N., Sumioka, C., Takeda, K., Izuta, T., 2014. Evaluation of the effects of ozone on yield of Japanese rice (*Oryza sativa* L.) based on stomatal ozone uptake. Environ. Pollut. 184, 472–480. https://doi.org/10.1016/j.envpol.2013.09.024.

Yang, W., Omaye, S.T., 2009. Air pollutants, oxidative stress and human health. Mutat. Res. 674, 45–54. https://doi.org/10.1016/j.mrgentox.2008.10.005.

Yarwood, G., Rao, S., Yocke, M., Whitten, G., 2005. Updates to the Carbon Bond Chemical Mechanism: CB05. Final report to the US EPA, RT-0400675.

Yu, S., Mathur, R., Sarwar, G., Kang, D., Tong, D., Pouliot, G., Pleim, J., 2010. Eta-CMAQ air quality forecasts for O_3 and related species using three different photochemical mechanisms (CB4, CB05, SAPRC-99): comparisons with measurements during the 2004 ICARTT study. Atmos. Chem. Phys. 10, 3001–3025. https://doi.org/10.5194/acp-10-3001-2010.

Zhang, Y., Wen, X.-Y., Wang, K., Vijayaraghavan, K., Jacobson, M.Z., 2009. Probing into regional O_3 and particulate matter pollution in the United States: 2. An examination of formation mechanisms through a process analysis technique and sensitivity study. J. Geophys. Res. 114, D22305.